

## H $\alpha$ EMISSION VARIABILITY IN ACTIVE M DWARFS

KEATON J. BELL<sup>1,2,\*</sup>, ERIC J. HILTON<sup>1,3</sup>, JAMES R. A. DAVENPORT<sup>1</sup>, SUZANNE L. HAWLEY<sup>1</sup>, ANDREW A. WEST<sup>4</sup>, AND ALLEN B. ROGEL<sup>5</sup>

*Received: 2011 November 30; Accepted: 2011 December 1*

### ABSTRACT

We use  $\sim 12,000$  spectra of  $\sim 3,500$  magnetically active M0-M9 dwarfs from the Sloan Digital Sky Survey taken at 10-15 minute intervals, together with  $\sim 300$  spectra of  $\sim 60$  M0-M8 stars obtained hourly with the Hydra multi-object spectrometer, to probe H $\alpha$  variability on timescales of minutes to weeks. With multiple observations for every star examined, we are able to characterize fluctuations in H $\alpha$  emission as a function of activity strength and spectral type. Stars with greater magnetic activity (as quantified by  $L_{H\alpha}/L_{bol}$ ) are found to be less variable at all spectral types. We attribute this result to the stronger level of persistent emission in the high activity stars, requiring a larger heating event in order to produce measurable variability. We also construct H $\alpha$  structure functions to constrain the timescale of variability. The more active objects with lower variability exhibit a characteristic timescale longer than an hour, likely due to larger, longer lasting heating events, while the less active objects with higher variability have a characteristic timescale shorter than 15 minutes.

*Subject headings:* stars: activity — stars: chromospheres — stars: flare — stars: low-mass — stars: magnetic fields

### 1. INTRODUCTION

M dwarfs, the least massive and most numerous stars in our Galaxy, provide remote laboratories for observing high-energy magnetic phenomena in stellar atmospheres. The red and dim nature of M dwarfs makes the H $\alpha$  spectral feature the most accessible tracer of magnetic activity in their convective outer layers (Bopp & Schmitz 1978; Walkowicz & Hawley 2009). M dwarfs with H $\alpha$  in emission are classified as magnetically active, with a greater fraction of stars showing H $\alpha$  emission at later spectral types (Hawley et al. 1996; Gizis et al. 2000; West et al. 2011). Magnetic activity is correlated with energetic flaring events that last seconds to hours (Moffett 1974; Kowalski et al. 2010) and photometric brightness increases as large as 8.2 magnitudes in the *B*-band (Almeida et al. 2011). The incidence of H $\alpha$  emission and large flares decreases for stars farther from the Galactic Plane (West et al. 2006, 2008; Kowalski et al. 2009; Hilton et al. 2010; Walkowicz et al. 2011). This is interpreted as an age effect, leading to activity timescales of 1–8 billion years for early–late M dwarfs respectively.

Variability in quiescent (non-flaring) H $\alpha$  emission has been attributed to both stellar rotation and M dwarf activity cycles. Bopp & Schmitz (1978) related sequential H $\alpha$  measurements to orbital phase and suggested that the observed changes were caused by the rotation of localized active regions in and out of view on timescales of

days. Activity cycles with periods of a few years have been identified for M dwarfs by Cincunegui et al. (2007) and Buccino et al. (2011), and may affect the observed strength of H $\alpha$  emission. Although large flares are relatively infrequent events (Hilton 2011), sporadic low-level magnetic field reconnection events (“microflares”) may also contribute to inherent H $\alpha$  emission variations in active M dwarfs.

There have been some recent investigations of H $\alpha$  variability on timescales of minutes to days. Gizis et al. (2002) measured the H $\alpha$  equivalent widths (EWHA) for a sample of more than 600 active M0–M6 dwarfs from the Palomar/Michigan State University (PMSU) survey of nearby stars (Reid et al. 1995), and found that the variation in repeated measurements was near 15% for stars with mean EWHA,  $\langle \text{EWHA} \rangle < 5\text{\AA}$ , while the variability for stars with  $\langle \text{EWHA} \rangle > 5\text{\AA}$  was in excess of 30%. In their study of EWHA variations on later type stars, Lee et al. (2010) identified significant variability in  $\sim 80\%$  of their sample of 43 M4–M8 stars. They found that the majority of variability events had timescales of 30 minutes or longer, and that the later-type stars were more variable, as measured by  $R(\text{EW}) = \max(\text{EWHA})/\min(\text{EWHA})$ . Similarly, Kruse et al. (2010) found an increase in the same metric (which they refer to as  $R_{EW}$ ) at later spectral types for timescales from 15 minutes to an hour in the Sloan Digital Sky Survey (SDSS; York et al. 2000) Data Release 7 (DR7; Abazajian et al. 2009) component spectra. They also noted that  $R_{EW}$  was larger for intermittent sources.

Our analysis uses a set of spectra with exposure times of  $\sim 1$  hour from the multi-object Hydra spectrograph on the WIYN telescope at Kitt Peak National Observatory, as well as the component spectra from SDSS, to extend the evaluation of H $\alpha$  variability using new metrics and a broader range of timescales. We employ a construct known as the structure function, which is commonly used

<sup>1</sup> Astronomy Department, University of Washington, Seattle, WA 98195

<sup>2</sup> Department of Astronomy, University of Texas, Austin, TX 78712

<sup>3</sup> Dept. of Geology and Geophysics and Institute for Astronomy, University of Hawaii at Manoa, Honolulu, HI 96822

<sup>4</sup> Department of Astronomy, Boston University, Boston, MA 02215

<sup>5</sup> Department of Physics & Astronomy, Bowling Green State University, Bowling Green, OH 43403

\* Direct correspondence to: keatonb@astro.as.utexas.edu

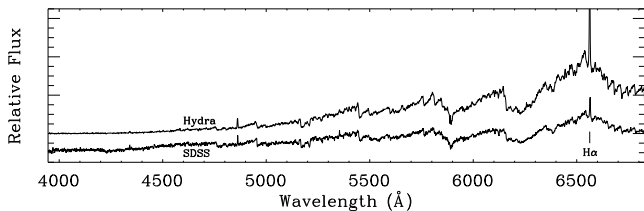


**Figure 1.** Sample high-S/N active M4 dwarf spectra from the Hydra (top) and SDSS (bottom) data are shown. The data have moderate spectral resolution (2000-4000) and wavelength coverage from  $\sim 4000$ - $9000\text{\AA}$  for SDSS and  $\sim 4000$ - $7000\text{\AA}$  for Hydra.

in quasar variability analyses (e.g. Simonetti et al. 1985; MacLeod et al. 2011), to further constrain the timescales of  $H\alpha$  emission variability.

The spectroscopic M dwarf samples we used are detailed in Section 2, along with our methods for determining spectral types and measuring  $H\alpha$  emission strength. Analysis of  $H\alpha$  emission variability with spectral type, activity strength and timescale is presented in Section 3, and we summarize our findings in Section 4.

## 2. DATA

Our data come from two sources that are discussed in detail below: the Hydra instrument on the WIYN telescope (Section 2.1), and the Sloan Digital Sky Survey (Section 2.2). Representative spectra from each sample are displayed in Figure 1. The spectral type distributions of the active M dwarfs in the two samples are shown in Figure 2. These moderate-resolution data sources (Hydra:  $R\sim 4000$ , SDSS:  $R\sim 2000$ ) are useful for our  $H\alpha$  variability analysis because they each provide multiple spectra of the same objects at well-defined time intervals.

### 2.1. WIYN Hydra Data

Our analysis employs data that were taken over 27 nights between January 2002 and July 2008 as part of the *Chandra* Multiwavelength Plane Survey (ChaM-Plane; Grindlay et al. 2005), which was designed to investigate the fraction of diffuse X-ray emission in the Galactic plane due to unresolved X-ray point sources. Candidate point sources were identified using *VRIH $\alpha$*  photometry obtained with the Mosaic cameras at the Cerro Tololo Inter-American Observatory and the Kitt Peak National Observatory 4-meter telescopes. Spectra were obtained with the Hydra multi-object fiber-fed spectrograph on the 3.5-meter WIYN telescope for objects with  $H\alpha - R < -0.3$ , indicating excess  $H\alpha$  emission, as well as optically detected objects with corresponding X-ray emission in archival *Chandra* images. Although the survey was designed to identify accretion powered sources such as cataclysmic variables and low-mass X-ray binaries, initial analysis by the ChaMPlane team (Rogel et al. 2006) revealed a sizable population of M dwarfs in the sample, whose spectra and photometry we utilize in this study.

We assigned spectral types to the Hydra data using the Hammer software (Covey et al. 2007) in manual mode, because the flux calibration and signal-to-noise ratio (typically  $\sim 10$ ) of the spectra, especially at blue wavelengths, did not allow automatic typing. Each object was visually compared to the Hammer set of M dwarf templates (Bochanski et al. 2007). The resulting spectral types are accurate to within 1–2 types. We verified

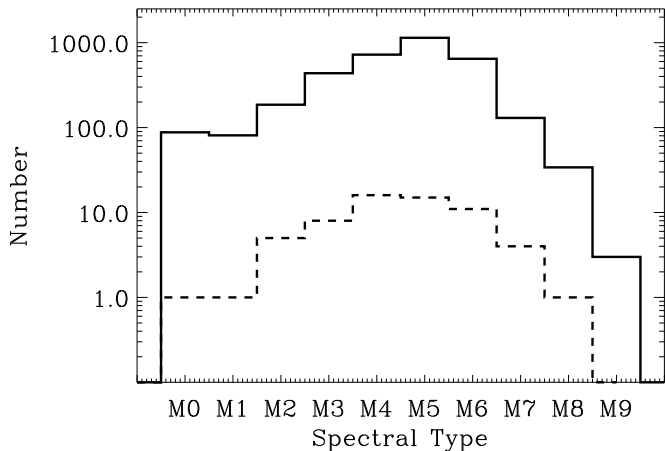


**Figure 2.** The distribution of spectral types is similar for the magnetically active M dwarfs in the SDSS (solid line) and Hydra (dashed line) samples.

that the spectral types were broadly consistent with the measured  $V - I$  colors of the objects.

The strength of  $H\alpha$  emission in each spectrum was quantified by measuring the equivalent width of the line. We followed the procedure described in West et al. (2004) and adopted their definitions for the  $H\alpha$  line and continuum regions. Figure 3 identifies these regions for the four Hydra spectra obtained for a representative M4 dwarf. We visually inspected every spectrum in the sample to ensure that the EWHA measurements were not contaminated by cosmic rays or other artificial defects.

Because the equivalent width is measured with respect to the local continuum level, it can be misleading to compare EWHA among stars of different spectral type, and hence continuum flux near  $H\alpha$ . We therefore computed the ratio of the  $H\alpha$  line luminosity to the bolometric luminosity ( $L_{H\alpha}/L_{bol}$ ) for each object using the  $\chi$  conversion factors of West & Hawley (2008). This quantity represents the continuum-independent activity level, which allows for  $H\alpha$  emission to be compared between stars of

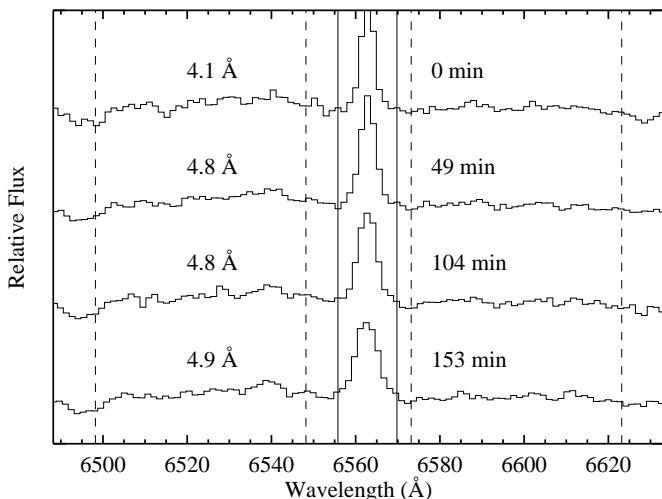


**Figure 3.**  $H\alpha$  line profiles in the Hydra data for repeated observations of an M4 dwarf. The solid vertical lines indicate the boundaries of the line region used in the equivalent width calculations, and the dashed lines mark the pseudo-continuum regions on either side. The measured equivalent width for each spectrum is indicated to the left of the emission line, and the time elapsed since the beginning of the first exposure is shown on the right.

different spectral types.

Our analysis was limited to the chromospherically active M dwarfs, identified by the criteria of West et al. (2011) that define detectable H $\alpha$  emission. Because we intend to use these data in a time-domain analysis, we further restricted the sample to include only those stars with at least three spectra that were identified as active. Our final Hydra sample contains 312 spectra from 62 active M0–M8 dwarfs, and allows us to probe H $\alpha$  emission variability on timescales from one to three hours.

## 2.2. SDSS Spectra

All SDSS spectra are composites of several (typically 3–5) spectra with  $\sim 10$ –15 minute exposure times. The individual component spectra (with typical signal-to-noise ratio  $\sim 7$ ) were initially made public as part of the SDSS Data Release 6 (DR6; Adelman-McCarthy et al. 2008). Previous studies have examined the spectral variability of M dwarfs using the individual SDSS spectra from DR6 (Hilton et al. 2010) and DR7 (Kruse et al. 2010); our analysis expands on these efforts. We use the Hilton et al. (2010) sample, which has the spectral type for each object assigned from the composite spectra presented in West et al. (2008). The EWHA measurements for the component spectra followed the same prescription as for the Hydra data.  $L_{H\alpha}/L_{bol}$  values were obtained from the EWHA calculated for each object, and we verified that they agreed with those measured from the composite spectra given in West et al. (2008). We further restricted our sample to include only the persistently active objects that showed measurable H $\alpha$  emission in every individual exposure. We note that this reduced the Hilton et al. (2010) active sample by less than 3%.

Our final SDSS sample consists of 11,989 spectra for 3,469 active M0–M9 dwarfs, and allows us to examine variability on timescales from  $\sim 15$ –100 minutes. Nearly 700 stars were observed on multiple days, allowing us to further probe H $\alpha$  emission changes on timescales of  $\sim 1$ –20 days.

## 3. VARIABILITY ANALYSIS AND RESULTS

We first consider H $\alpha$  variability as a function of spectral type, comparing our results with variability indicators used in previous analyses (Section 3.1). Our preferred metric for variability is  $\sigma_{EWHA}/\langle EWHA \rangle$ , and we investigate this metric as a function of activity strength ( $L_{H\alpha}/L_{bol}$ ; Section 3.2). Finally, we compute structure functions to investigate characteristic timescales in the low- and high-variability subsets of our data (Section 3.3).

### 3.1. H $\alpha$ Variability with Spectral Type

Lee et al. (2010) and Kruse et al. (2010) both found that H $\alpha$  variability increases at later spectral type, using the  $R_{EW}$  metric. Figure 4 illustrates  $R_{EW}$  as a function of spectral type for our Hydra and SDSS samples. In agreement with their analyses, we find that the distributions are not symmetric, but have significant extensions to large values of  $R_{EW}$ , with these extensions being more pronounced at later spectral type. However, in our samples the median values (the median is preferred as a statistic instead of the mean for these skewed distributions) scatter around a roughly constant value. This

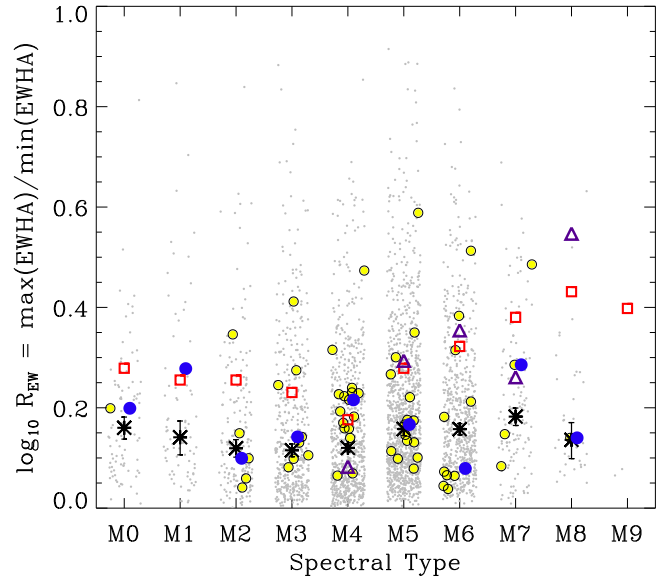


**Figure 4.** The  $R_{EW}$  variability metric is shown as a function of spectral type for the SDSS data (light gray dots) and Hydra data (light blue diamonds), illustrating distributions with large numbers of low-variability objects and extended tails toward higher variability that are more noticeable at later types. The distributions are artificially broadened at each spectral type to more clearly show the actual number of objects. The median of each type is given by the black asterisks (SDSS) and blue filled circles (Hydra). There is no obvious trend in the medians with spectral type. The red squares and purple triangles denoting results from Kruse et al. (2010) and Lee et al. (2010) respectively, are shown for comparison. See text for discussion.

is in contrast to the Kruse et al. (2010) and Lee et al. (2010) results, shown as red squares and purple triangles respectively. We attribute the difference to the criteria used to identify the active stars. Kruse et al. (2010) and Lee et al. (2010) include stars that they characterize as “intermittently” variable (i.e. only showing H $\alpha$  emission in a subset of their spectra), and they exclude weakly active stars, which they classify as inactive. These differ from our analysis as a result of their non-uniform equivalent width measurement criteria. Their intermittently variable stars are more prevalent at later types and systematically exhibit larger values of the  $R_{EW}$  metric. We are able to confidently identify H $\alpha$  at much smaller equivalent width, even in late-type M dwarfs, provided the spectra have sufficiently high signal-to-noise ratios (West et al. 2008). Evidently, including these less active, but persistent, objects leads to the approximately flat distribution outlined by the SDSS and Hydra medians in Figure 4.

### 3.2. H $\alpha$ Variability with Activity Strength

Gizis et al. (2002) used the standard deviation of repeated EWHA measurements ( $\sigma_{EWHA}$ ) for each star as a metric for line strength variability, and found that this value increased with  $\langle EWHA \rangle$  for their sample. We investigate that result in Figure 5a, which illustrates the variation of  $\sigma_{EWHA}$  with  $\langle EWHA \rangle$  for stars in both the Hydra and SDSS samples. The median  $\sigma_{EWHA}$  for bins containing roughly equal numbers of stars are also shown. The abrupt cutoff at  $\langle EWHA \rangle \sim 1\text{\AA}$  is due to our requirements for measurable H $\alpha$  equivalent width in these data (West et al. 2008).

We see that the median  $\sigma_{EWHA}$  is near zero for low

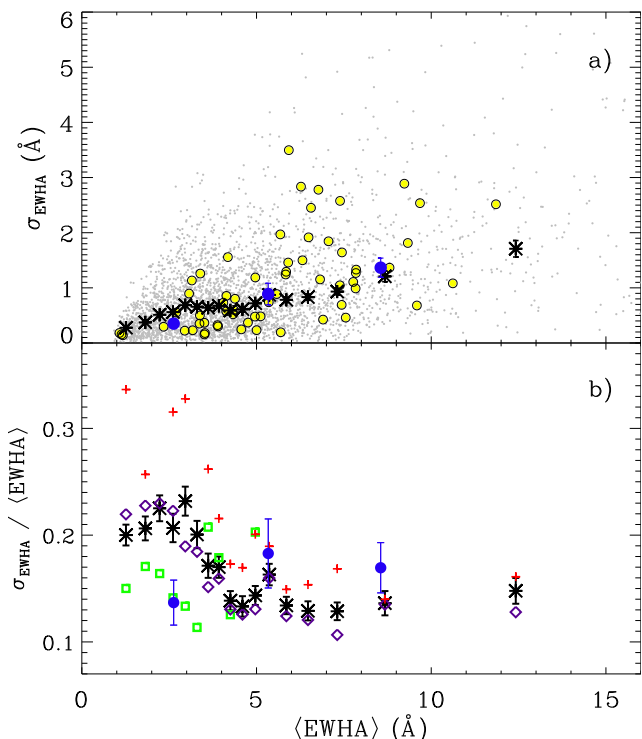


**Figure 5.** a) The standard deviation in EWHA ( $\sigma_{EWHA}$ ) versus mean EWHA ( $\langle EWHA \rangle$ ) is shown for each star in the Hydra and SDSS samples. Medians of representative bins are also shown (black asterisks for SDSS, blue circles for Hydra). There is a rising trend toward larger  $\sigma$  and higher scatter as  $\langle EWHA \rangle$  increases. b) The medians of the binned data for the fractional variability metric  $\sigma_{EWHA}/\langle EWHA \rangle$  are shown grouped by spectral type for the SDSS data (M0–M2 as green squares, M3–M5 as purple diamonds and M6–M9 as red crosses). There is a clear separation by spectral type, and a general decreasing trend toward lower variability at larger  $\langle EWHA \rangle$ . The median SDSS and Hydra data have the same symbols as in the top panel.

$\langle EWHA \rangle$ , rising to  $\sim 0.8\text{\AA}$  at  $\langle EWHA \rangle \sim 3\text{--}6\text{\AA}$  and increasing to  $\sim 1.8\text{\AA}$  at  $\langle EWHA \rangle > 10\text{\AA}$ . Our well-sampled data show a smooth, continuously increasing scatter of  $\sigma_{EWHA}$  with  $\langle EWHA \rangle$  for the median points, in qualitative agreement with the much smaller sample of Gizis et al. (2000). We also note that the maximum value of  $\sigma_{EWHA}$  increases with  $\langle EWHA \rangle$ .

As noted above, the absolute equivalent width values depend on spectral type due to the changing continuum flux near  $H\alpha$ , with earlier type stars having relatively smaller equivalent width due to their higher continuum flux. We illustrate this effect in Figure 5b using the fractional variability metric  $\sigma_{EWHA}/\langle EWHA \rangle$ . The skewed nature of the  $\sigma$  distributions at a given  $\langle EWHA \rangle$ , evident in Figure 5a (and analogous to the skewed distributions in  $R_{EW}$  shown in Figure 4), again leads us to use the median value to characterize  $\sigma_{EWHA}/\langle EWHA \rangle$  for each  $\langle EWHA \rangle$  bin.

The spectral type dependence of  $\langle EWHA \rangle$  is clearly indicated by the separation of the early (M0–M2, green squares), mid (M3–M5, purple diamonds) and late (M6–M9, red crosses) types for the SDSS sample. The median  $\sigma_{EWHA}/\langle EWHA \rangle$  values for all spectral types are shown as black asterisks (SDSS) and blue filled circles (Hydra). The variability metric decreases with increasing  $\langle EWHA \rangle$  from  $\sim 0.2$  for stars with low EWHA to  $\sim 0.14$  for stars with  $\langle EWHA \rangle > 5\text{\AA}$ .

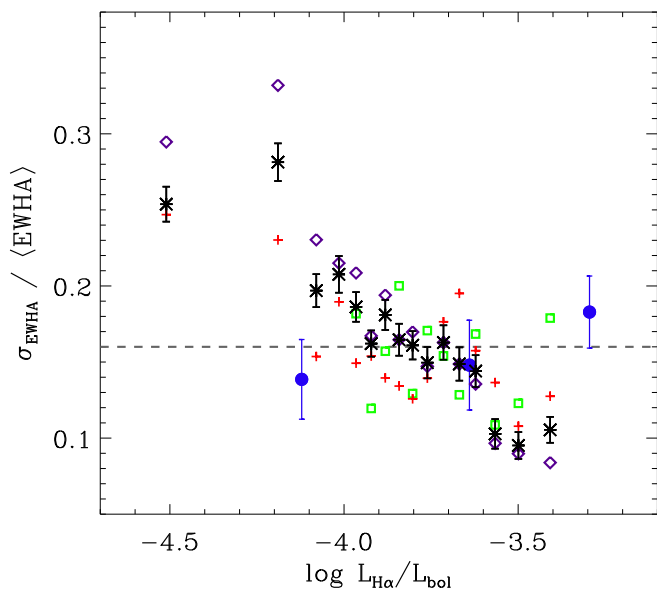


**Figure 6.** The same medians of the fractional variability metric ( $\sigma_{EWHA}/\langle EWHA \rangle$ ) from Figure 5b are shown as a function of activity strength  $\log L_{H\alpha}/L_{bol}$ . The symbols are the same as in Figure 5b. The downward trend in the SDSS data shows that variability decreases in more active M dwarfs, regardless of spectral type. The Hydra data do not show a coherent trend, which we attribute to poor sampling and a bias toward very active, early type stars.

A better measure of magnetic activity strength that accounts for the continuum dependence on spectral type is  $L_{H\alpha}/L_{bol}$ . Figure 6 illustrates the same fractional variability metric  $\sigma_{EWHA}/\langle EWHA \rangle$  as in Figure 5b, versus activity strength. The spectral types are no longer separated; in fact the three spectral type groups from Figure 5b, have shifted horizontally so that they now overlap and form a smooth distribution. It is clear that the underlying variability relationship is not a function of spectral type but rather of activity strength. However, the median fractional variability (black asterisks) decreases with increasing activity from  $\sim 0.3$  at  $\log(L_{H\alpha}/L_{bol}) \sim -4.5$  to  $\sim 0.1$  at  $\log(L_{H\alpha}/L_{bol}) \sim -3.5$ . The median value for the variability metric across the entire sample is 0.16, shown as the dashed line on the Figure.

The Hydra data (blue filled circles) in Figures 5b and 6 show relatively flat distributions that are influenced by small numbers, uneven spectral type sampling, and a bias toward very active stars especially at early spectral types (due to the  $H\alpha - R$  color selection of the targets). Therefore, they are not as useful as the SDSS data for understanding the behavior of the variability metric with activity strength.

The picture we have developed is that highly active stars of all spectral types are relatively less variable than low activity stars. This only becomes evident when the well-known underlying relationship between activity strength and spectral type is removed, as in Figure 6. Physically, the strong level of persistent emission in the high activity stars may be due to a large surface coverage of active regions, while the low activity stars may have a relatively smaller filling factor. An increase in  $H\alpha$  emission, for example due to a new active region appearing on the surface, or a magnetic heating episode or microflare in one of the existing active regions, will then manifest as barely visible in the more active star, while it

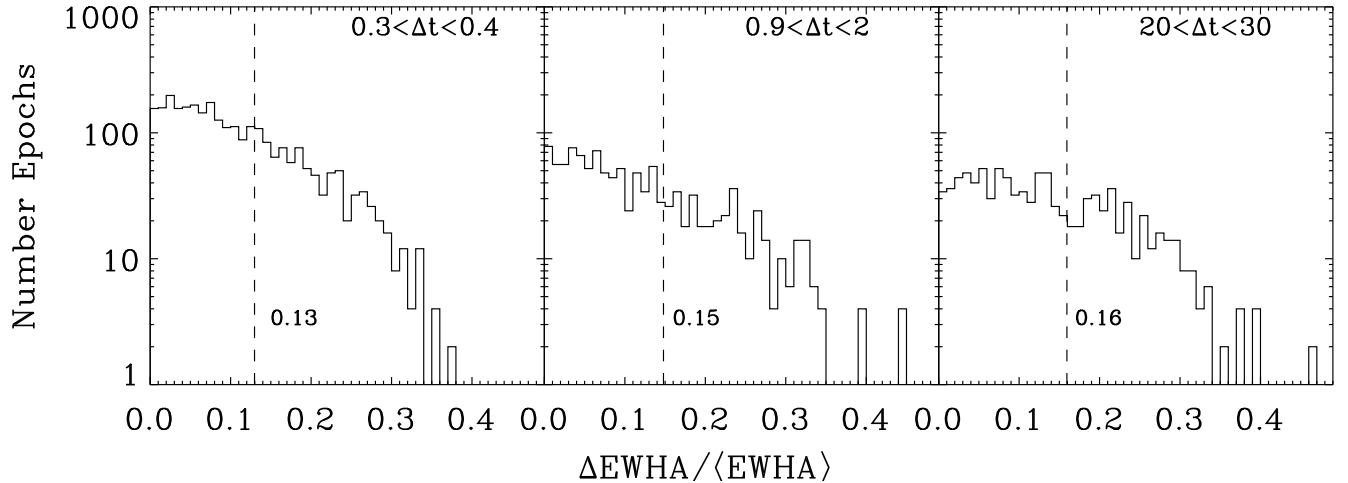


**Figure 7.** Three time bins from the structure function of the low-variability SDSS sources. Each point on the structure function in Figure 8 is a normalized RMS (denoted by the vertical dashed lines) calculated from a distribution of  $\Delta EWHA/\langle EWHA \rangle$  that is populated by pairs of observations separated by a specific range of time,  $\Delta t$  (given in hours at the top of each panel).

will contribute significant new emission in the less active star. This would naturally explain why the less active stars are relatively more variable.

### 3.3. Structure Functions and Timescales of H $\alpha$ Variability

Structure functions are often used to explore the variability timescales present in time-resolved observations of quasars (e.g. Simonetti et al. 1985; MacLeod et al. 2011). They represent the change observed between two measurements of some variable quantity, typically broadband flux in the case of quasars, as a function of the time between measurements ( $\Delta t$ ). It is expected that if the observed variability operates on a characteristic timescale ( $\tau$ ), then for  $\Delta t < \tau$ , the measurements will be correlated. The variability amplitude will increase with greater time separation as the observations sample more of the total variability range until  $\Delta t = \tau$ . For  $\Delta t > \tau$ , the structure function maintains a constant amplitude as the measurements are uncorrelated and randomly sample the full variability range.

We employ structure functions here to quantify the typical change in the equivalent width measurements for active M dwarf spectra in many bins of time separation,  $\Delta t$ , and to constrain the characteristic timescale of variability,  $\tau$ . We divide our samples at the median value of the fractional variability metric in Figure 6 into the less active but more-variable stars ( $\sigma_{EWHA}/\langle EWHA \rangle > 0.16$ ), and the more active but less-variable stars ( $\sigma_{EWHA}/\langle EWHA \rangle < 0.16$ ). We then calculate the change in H $\alpha$  emission as a fraction of the mean value,  $\Delta EWHA/\langle EWHA \rangle$ , between every pair of repeated measurements for the same M dwarf.

To illustrate how the structure function amplitude is calculated, the distributions for three SDSS time bins from the less-variable (more active) subsample are presented in Figure 7. Each time bin (the  $\Delta t$  range indicated on the Figure) contributes one point on the structure function. The typical change between measurements for a given  $\Delta t$  bin is taken as the RMS of the  $\Delta EWHA/\langle EWHA \rangle$  distribution, normalized by the number of samples in that time bin. This accounts for the uneven sampling of time separations in our datasets.

The normalized RMS values for these three bins increase from 0.13 to 0.16 with increasing  $\Delta t$ . The SDSS structure functions were constructed from similar normalized RMS values that were calculated for 14 time bins spanning the entire range of  $\Delta t$  sampled by our data. The time bins were chosen to provide good statistics at short  $\Delta t$  intervals (15 minutes to 2 hours), where there are many observations, and to cluster around typical  $\Delta t$  values for longer intervals (e.g. one day, several days). The Hydra structure functions were only computed for a few time intervals, reflecting the approximately hourly cadence of the observations.

Figure 8a illustrates the SDSS (black asterisks) and Hydra (blue filled circles) structure functions for the high-variability sample ( $\sigma_{EWHA}/\langle EWHA \rangle > 0.16$ ), and Figure 8b gives the structure functions for the low-variability sample ( $\sigma_{EWHA}/\langle EWHA \rangle < 0.16$ ). The timescales range from 15 minutes to 20 days. The irregular binning in  $\Delta t$  reflects the non-uniform separations of the measurements in time due to the sampling cadences of the surveys. We also require that the shortest time bins ( $\Delta t < 2$  hours) in the SDSS structure function contain at least 150 measurement pairs, in order to obtain well-defined normalized RMS values (see Figure 7). At larger time separations, the sample sizes are smaller and the error bars on the structure function amplitudes are correspondingly larger.

The low-variability structure function for the SDSS sample in Figure 8b shows a significant trend with time, indicating increasing variability up to a timescale of at least an hour. The plateau at timescales shorter than  $\Delta t \sim 0.4$  hours suggests that measurement uncertainties may dominate any variability amplitude effects below that time separation.

The high-variability structure function (Figure 8a), on the other hand, shows a flat distribution at all times for the SDSS sample. The structure function amplitude is much larger, which is indicative of the higher level of variability seen in this sample. The measurement uncertainties are much less than the detected RMS (structure function amplitude), indicating that the variability timescale is shorter than our smallest time separation bin,  $\sim 15$  minutes.

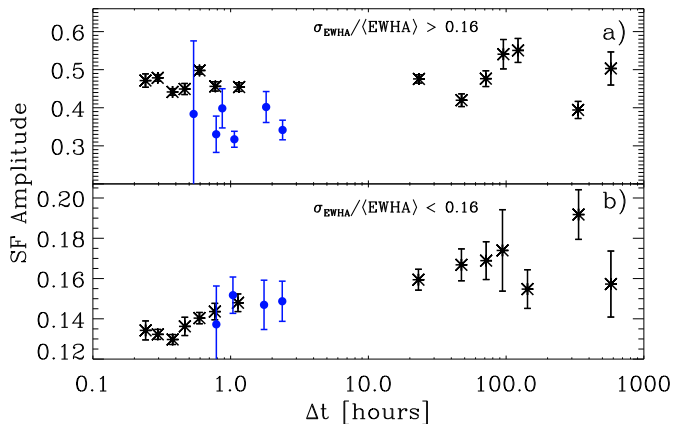


**Figure 8.** The structure functions for a) the high-variability (less active) stars; and b) the low-variability (more active) stars, for the SDSS (black asterisks) and Hydra (blue filled circles) samples. The low-variability stars show an increasing structure function amplitude between 0.4-1 hour, indicating a timescale of more than an hour for the variability. The high-variability stars apparently vary on timescales shorter than our smallest time separation ( $\sim 15$  minutes). The Hydra data are discussed separately in the text.

While sparsely sampled, the Hydra data reinforce this interpretation. In Figure 8a, both the SDSS and Hydra exposure times are longer than the underlying characteristic timescale for the high-variability data, and therefore all measurement pairs are randomly sampling the intrinsic equivalent width variations, leading to flat structure function amplitudes. The longer exposure time for the Hydra data (an hour compared to 10-15 minutes for SDSS) damps the stochastic variations between exposures, and the amplitude of the Hydra structure function is correspondingly smaller. The low-variability Hydra sample in Figure 8b has a characteristic timescale that is apparently comparable to the exposure time, and thus the structure function amplitude is flat over the 1–3 hour time separations that are sampled. In this case, the structure function amplitude is consistent between the SDSS and Hydra samples.

The increase in variability amplitude with time seen in our low-variability (high activity) sample is reminiscent of the Lee et al. (2010) result that there was a much larger number of  $H\alpha$  emission events that lasted at least 30 minutes compared to the number of shorter events they observed. Their sample was primarily composed of very active stars which is comparable to this subset of our data.

Following the discussion in §3.2, we interpret the timescale results as follows. The low-variability (high activity) stars are covered with spots, so that small variations are not easily visible against the high background. In order to see a noticeable variation, a rather significant event must occur. Since higher-energy events are known to last longer (e.g. Lacy et al. 1976; Hawley & Pettersen 1991), this leads to a longer timescale for events that are strong enough to be detected above the persistent activity. For the high-variability (low activity) stars, small events will cause a noticeable change, and these occur on short timescales, below the  $\sim 15$  minute limit of our sampling cadence.

#### 4. SUMMARY

We used two spectroscopic samples of active M dwarfs to examine  $H\alpha$  emission variability on timescales from

minutes to weeks.

We found that the  $H\alpha$  variability measured using the  $R_{EW}$  metric remains relatively constant as a function of spectral type, in contrast to previous results. However, using our fractional variability metric ( $\sigma_{EWHA}/\langle EWHA \rangle$ ), we showed that the higher-variability stars have relatively low activity strength ( $L_{H\alpha}/L_{bol}$ ), and conversely the low-variability stars have high activity strength. This naturally leads to an apparent dependence on spectral type because the later type stars typically have lower activity strength. We speculated that the physical reason for the higher variability in the low activity stars is that small changes in  $H\alpha$  emission, e.g. due to small-scale flaring or the appearance of a new active region on the stellar surface, would have a relatively larger effect on the less active stars.

We investigated the timescales of  $H\alpha$  emission variability using structure functions. The observed  $H\alpha$  variations for low-variability stars ( $\sigma_{EWHA}/\langle EWHA \rangle < 0.16$ ) occur on a timescale longer than an hour, while the high-variability M dwarfs exhibit a timescale that is shorter than our sampling time of  $\sim 15$  minutes. Neither the low nor high variability samples show significant changes in the structure function on timescales longer than a day. We speculated that the low-variability sample, which is mainly composed of the higher activity strength stars, requires more energetic and hence longer-lived emission events in order to be detected above the strong persistent surface activity, leading to a longer characteristic variability timescale.

Better time resolution in spectroscopic M dwarf monitoring, as well as a wider and better-sampled range of time separations, will allow for a more accurate determination of the timescales of  $H\alpha$  variability in low-mass dwarfs and may lead to a better understanding of the physical mechanisms that cause these changes.

We acknowledge NSF grant AST 08-07205, and thank David Schlegel for help obtaining the individual component SDSS spectra.

Funding for the SDSS and SDSS-II has been provided by the Alfred P. Sloan Foundation, the Participating Institutions, the National Science Foundation, the U.S. Department of Energy, the National Aeronautics and Space Administration, the Japanese Monbukagakusho, the Max Planck Society, and the Higher Education Funding Council for England. The SDSS Web site is <http://www.sdss.org/>. The SDSS is managed by the Astrophysical Research Consortium for the Participating Institutions. The Participating Institutions are the American Museum of Natural History, Astrophysical Institute Potsdam, University of Basel, University of Cambridge, Case Western Reserve University, University of Chicago, Drexel University, Fermilab, the Institute for Advanced Study, the Japan Participation Group, Johns Hopkins University, the Joint Institute for Nuclear Astrophysics, the Kavli Institute for Particle Astrophysics and Cosmology, the Korean Scientist Group, the Chinese Academy of Sciences (LAMOST), Los Alamos National Laboratory, the Max-Planck Institute for Astronomy (MPIA), the Max-Planck Institute for Astrophysics (MPA), New Mexico State University, Ohio State University, University of Pittsburgh, University of Portsmouth, Princeton University, the United States Naval Observatory, and the University of Washington.

## REFERENCES

- Abazajian, K. N., et al. 2009, *ApJS*, 182, 543  
Adelman-McCarthy, J. K., et al. 2008, *ApJS*, 175, 297  
Almeida, L. A., Jablonski, F., & Martioli, E. 2011, *A&A*, 525, A84+
- Bochanski, J. J., West, A. A., Hawley, S. L., & Covey, K. R. 2007, *AJ*, 133, 531  
Bopp, B. W., & Schmitz, M. 1978, *PASP*, 90, 531  
Buccino, A. P., Díaz, R. F., Luoni, M. L., Abrevaya, X. C., & Mauas, P. J. D. 2011, *AJ*, 141, 34  
Cincunegui, C., Díaz, R. F., & Mauas, P. J. D. 2007, *A&A*, 461, 1107  
Covey, K. R., et al. 2007, *AJ*, 134, 2398  
Gizis, J. E., Monet, D. G., Reid, I. N., Kirkpatrick, J. D., Liebert, J., & Williams, R. J. 2000, *AJ*, 120, 1085  
Gizis, J. E., Reid, I. N., & Hawley, S. L. 2002, *AJ*, 123, 3356  
Grindlay, J. E., et al. 2005, *ApJ*, 635, 920  
Hawley, S. L., Gizis, J. E., & Reid, I. N. 1996, *AJ*, 112, 2799  
Hawley, S. L., & Pettersen, B. R. 1991, *ApJ*, 378, 725  
Hilton, E. J. 2011, PhD thesis, University of Washington  
Hilton, E. J., West, A. A., Hawley, S. L., & Kowalski, A. F. 2010, *AJ*, 140, 1402  
Kowalski, A. F., Hawley, S. L., Hilton, E. J., Becker, A. C., West, A. A., Bochanski, J. J., & Sesar, B. 2009, *AJ*, 138, 633  
Kowalski, A. F., Hawley, S. L., Holtzman, J. A., Wisniewski, J. P., & Hilton, E. J. 2010, *ApJ*, 714, L98  
Kruse, E. A., Berger, E., Knapp, G. R., Laskar, T., Gunn, J. E., Loomis, C. P., Lupton, R. H., & Schlegel, D. J. 2010, *ApJ*, 722, 1352  
Lacy, C. H., Moffett, T. J., & Evans, D. S. 1976, *ApJS*, 30, 85  
Lee, K., Berger, E., & Knapp, G. R. 2010, *ApJ*, 708, 1482  
MacLeod, C. L., et al. 2011, *ApJ*, 728, 26  
Moffett, T. J. 1974, *ApJS*, 29, 1  
Reid, I. N., Hawley, S. L., & Gizis, J. E. 1995, *AJ*, 110, 1838  
Rogel, A. B., Lugger, P. M., Cohn, H. N., Slavin, S. D., Grindlay, J. E., Zhao, P., & Hong, J. 2006, *ApJS*, 163, 160  
Simonetti, J. H., Cordes, J. M., & Heeschen, D. S. 1985, *ApJ*, 296, 46  
Walkowicz, L. M., et al. 2011, *AJ*, 141, 50  
Walkowicz, L. M., & Hawley, S. L. 2009, *AJ*, 137, 3297  
West, A. A., Bochanski, J. J., Hawley, S. L., Cruz, K. L., Covey, K. R., Silvestri, N. M., Reid, I. N., & Liebert, J. 2006, *AJ*, 132, 2507  
West, A. A., & Hawley, S. L. 2008, *PASP*, 120, 1161  
West, A. A., Hawley, S. L., Bochanski, J. J., Covey, K. R., Reid, I. N., Dhital, S., Hilton, E. J., & Masuda, M. 2008, *AJ*, 135, 785  
West, A. A., et al. 2004, *AJ*, 128, 426  
—. 2011, *AJ*, 141, 97  
York, D. G., et al. 2000, *AJ*, 120, 1579